Crystallized Mesoporous Ta-Nb Oxide

Crystallization of an Ordered Mesoporous Nb–Ta Oxide**

*Tokumitsu Katou, Byongjin Lee, Daling Lu, Junko N. Kondo, Michikazu Hara, and Kazunari Domen**

The preparation and application of mesoporous materials has been in recent years extended from silica-based materials to general inorganic materials such as oxides, sulfides and metals.[1] Applications now include catalysis, sorption, and

[*] Prof. K. Domen, T. Katou, Dr. J. N. Kondo, Prof. M. Hara
Chemical Resources Laboratory
Tokyo Institute of Technology, 4259
Nagatsuta-cho, Midori-ku, Yokohama, 226-8503 (Japan)
Fax: (+81) 45-924-5282
E-mail: kdomen@res.titech.ac.jp
Prof. K. Domen, Dr. B. Lee, Dr. D. Lu
Core Research for Evolutional Science and Technology (CREST)
Japan Science and Technology (Japan)

[**] This work was supported by the Core Research for Evolutional Science and Technology (CREST) program of the Japan Science and Technology (JST) Corporation.

Supporting information for this article is available on the WWW under http://www.angewandte.org or from the author.

  DOI: 10.1002/ange.200250263

sensing, as well as nano devices. In particular, mesoporous transition-metal oxides are expected to be useful functional inorganic materials with a wide range of potential applications.[2] For example, mesoporous Ta_2O_5[3] and Mg–Ta mixed oxide[4] exhibit high photocatalytic activity for the decomposition of water into H_2 and O_2 under ultraviolet irradiation, and mesoporous SnO_2 with a uniform pore size has been investigated as a gas sensor.[5] The amorphous pore walls of most mesoporous materials, which offer only poor thermal and mechanical stability, restrict the range of applications of these materials; whereas a crystallized wall structure can be expected to provide better thermal and mechanical stability as well as superior electric and optical properties. The crystallization and crystallinity of mesoporous materials have therefore attracted much attention. Hybrid mesoporous materials (HMMs), prepared from alkoxysilane $(CH_3CH_2O)_3Si{-}C_6H_4{-}Si(OCH_2CH_3)_3$ and with a 2D hexagonal mesoporous structure, were recently reported to have periodically ordered phenyl groups.[6] The synthesis of mesoporous zeolite single-crystals has also been reported.[7] We reported the preparation of crystallized mesoporous Nb–Ta oxide (NbTa-TIT-1) consisting of single-crystal particles forming a wormholelike mesoporous structure.[8] This Nb–Ta oxide exhibits remarkable hydrothermal and mechanical stability, and the preparation of single-crystal particles in an ordered mesoporous structure would be of significant interest. We successfully synthesized a Nb–Ta mixed oxide with 2D hexagonally ordered mesoporous structure,[9] and attempted the preparation of a crystallized wall structure. However, the material obtained consisted of crystallized particles in a wormholelike mesoporous structure, which suggests that the wormhole structure is formed during crystallization regardless of the structure of the amorphous precursor. The pore diameter increases from 6 to 13 nm and the wall thickness remains widely distributed (4–8 nm) after crystallization, suggestive of considerable mass transfer during the process. These findings appear to indicate that it is difficult to preserve the original ordered mesoporous structure after crystallization by simple calcination in air.[10]

Nanoporous carbon materials were prepared from various mesoporous silica templates.[11] Recently, as one of the advanced applications, it was reported that highly ordered mesoporous silica can be regenerated from nanoporous carbon materials.[12] As such carbon materials exhibit excellent thermal stability in inert atmospheres.[11] Mesopores of ordered mesoporous Nb–Ta oxide filled with carbon may offer a means of preserving the ordered mesoporous structure during crystallization. We have examined this possibility by filling the mesopores of 2D hexagonally ordered Nb–Ta oxide with carbon prior to crystallization. The results of crystallization are presented herein.

Figure 1 shows a typical transmission electron microscopy (TEM) image and electron diffraction (ED) pattern (inset) of the 2D hexagonally ordered mesoporous Nb–Ta oxide, which was used as an amorphous precursor for crystallization. The preparation method was reported in detail previously.[9] The ordered mesoporous Nb–Ta oxide was then crystallized following the procedure shown in Figure 2. After crystallization, a peak attributed to an ordered mesoporous structure

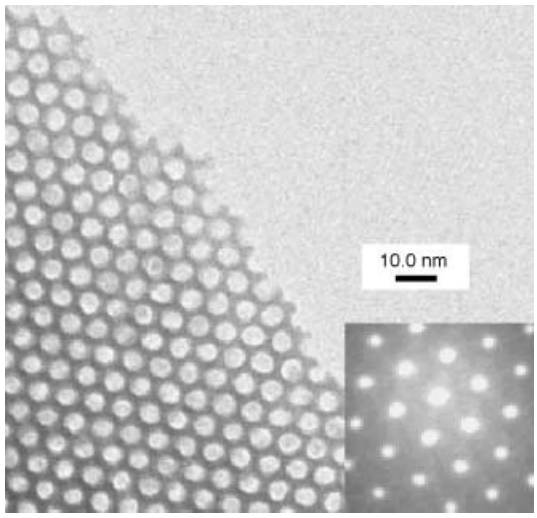

Figure 1. Representative TEM image and ED pattern (inset) of 2D hexagonally ordered mesoporous Nb–Ta oxide.

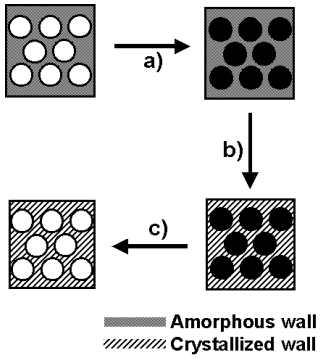

Figure 2. Conceptual scheme of the synthesis of mesoporous Nb–Ta oxide with 2D hexagonally ordered mesoporous structure and crystallized wall structure. a) Accumulation of polymerized furfuryl alcohol and subsequent carbonization at 823 K in vacuo. b) Crystallization of walls at 923 K under He. c) Removal of carbon by calcination at 773 K in air.

(d spacing = 6.8 nm) was observed in the powder X-ray diffraction (XRD) pattern (Figure 3). Wide-angle powder XRD revealed that a completely crystallized oxide phase, similar to that of NbTa-TIT-1[10], was prepared by calcination

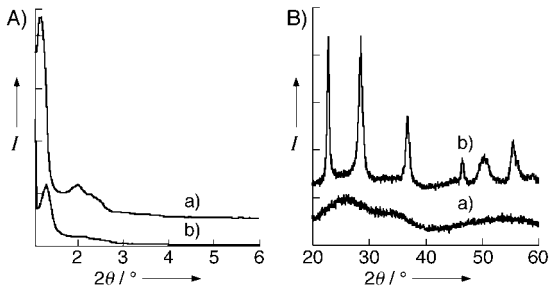

Figure 3. A) Low- and B) wide-angle powder XRD patterns a) before and b) after crystallization of 2D hexagonally ordered mesoporous Nb-Ta oxide. I = intensity, arbitrary units.

of the Nb–Ta oxide in air. The detailed assignment of peaks in the wide-angle powder XRD pattern has also been given in a previous report.[8] These results imply the presence of both an ordered mesoporous structure and crystallized walls. Figure 4a shows the TEM image of a particle with 2D hexagonally ordered mesopore channels, having somewhat curved lines. The ED pattern for the whole particle consists of mixed spots on a ring pattern. As the size of the single-crystal domain is not clear from Figure 4, ED patterns were obtained for smaller areas. Figure 4b) is a TEM image in a 100 nm

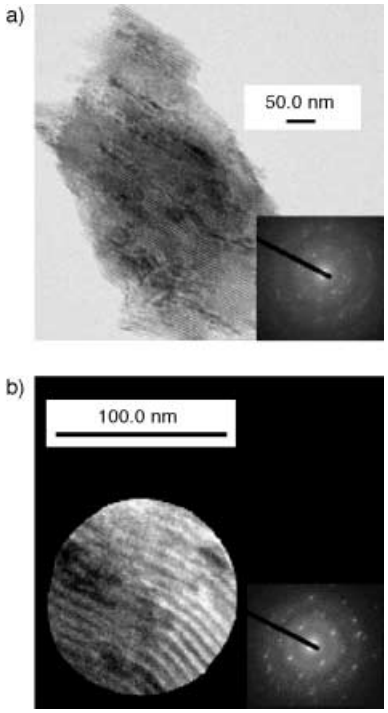

Figure 4. Typical TEM and ED analyses of NbTa-TIT-2. a) Image and ED pattern (inset) of a whole particle. b) Image and ED pattern (inset) of single-crystal domain of 100 nm.

region with corresponding ED pattern (inset). The observed mesoporous region consists of a single crystalline domain. The presence of mesopores in a single-crystal domain can be directly observed in high-resolution (HR) TEM images. As indicated by the arrows in the inset of Figure 5a and b, the lattice fringes extend coherently across several mesopores, thus confirming the existence of mesopores in a single-crystal domain. Figure 5a and b, taken for the same particle, reveal different directions of lattice fringes. This is consistent with the fact that there are several single-crystal domains in a particle. In the HRTEM image taken along the pore channel axis (Figure 5c) lattice fringes can be seen in the walls around pores with almost the same size and arrangement of mesopores as prior to crystallization. From these results, the mixed spot ED pattern (Figure 4a inset) is attributable to the presence of several single-crystal domains in the particle within an ordered mesoporous structure. From energy-dispersive X-ray spectroscopy (EDX) analysis, an Nb/Ta ratio of about one was confirmed at approximately 10 points

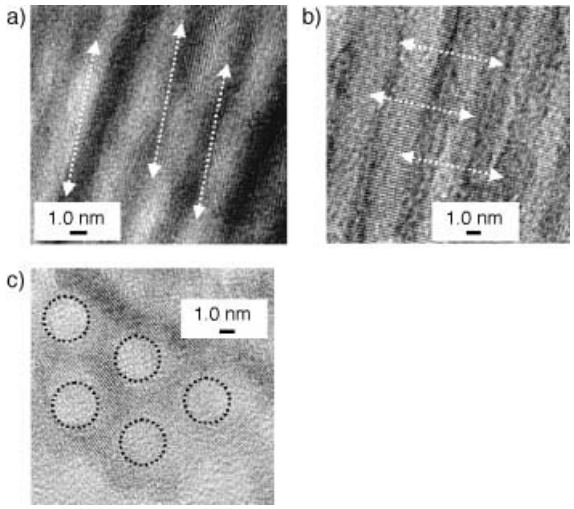

Figure 5. HRTEM images of NbTa-TIT-2. a) And b) lattice fringes in different orientations with respect to the pore channel direction. c) Lattice fringes on walls, viewed perpendicular to the pore channel axis.

(< ca. 5 nm size) on a particle in Figure 3a. This material is denoted NbTa-TIT-2, and represents a material obtained from a carbon-filled amorphous precursor with a 2D hexagonally ordered mesoporous structure.

The role of carbon in the preservation of the mesoporous structure was also examined. In the case of crystallization under helium at 923 K for 1 h in the absence of a carbon template, no peak was observed in the low 2θ region (1–6°) of the XRD results, and an N_2 uptake owing to the mesopores appeared at a relative pressure of around $P/P_0 = 0.8$ ($P_0 = 1 \times 10^5$ Pa). These results represent the physicochemical changes of NbTa-TIT-1 with the wormhole mesoporous structure, and differs markedly from the results for NbTa-TIT-2. Therefore, NbTa-TIT-2 cannot be constructed by calcination under helium without a carbon template. The mesoporous structure appears to be stabilized by the carbon template, thus preventing the structural change from a 2D hexagonal to a wormhole structure during crystallization.

According to the results shown in Figure 6, the N_2 uptake at $P/P_0 = 0.5$–0.7 for NbTa-TIT-2 is approximately a quarter of that of the amorphous precursor. The N_2 uptake at $P/P_0 = 0.8$ is derived from large pores, which increases markedly in size after crystallization of the amorphous precursor. In addition, the mesopore volume per gram decreases from 0.34 to 0.23 $mL\,g^{-1}$, probably owing to the collapse of mesopores. Therefore, approximately three quarters of the original mesopores (ca. 6.0 nm) of the amorphous precursor either are converted to larger pores or collapse after crystallization. Crystal domains with lower pore-wall periodicity are also observed by HRTEM. From the results obtained by XRD, N_2 isotherm and TEM image (see Supporting Information) before the removal of carbon (after crystallization of the pore walls), we regard the insufficient carbon content inside the pores of the sample as one of the reasons for the low yield of NbTa-TIT-2. Despite this low yield, the carbon templating method is still effective for controlling the mesoporous structure of crystallized mesoporous materials.

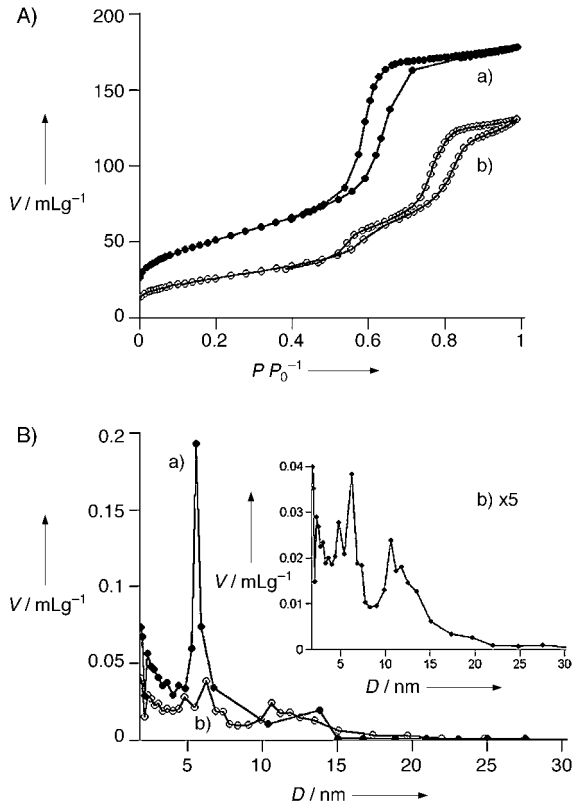

Figure 6. A) N_2 sorption isotherms and B) pore size distributions a) before and b) after crystallization of 2D hexagonally ordered mesoporous Nb–Ta oxide. V = volume of N_2 per gram of material.

Experimental Section

Two-dimensional hexagonal mesoporous Nb–Ta oxide, the amorphous precursor for crystallization, was synthesized based on a reported procedure.[9] The pore wall crystallization method is shown in Figure 2. Furfuryl alcohol vapor (0.023 mol h^{-1}) in nitrogen gas (30 mL min^{-1}) was passed through the amorphous precursor fixed in a reactor at 473 K for 2 h. The brown color of the resulting sample arises from the accumulation of polymerized furfuryl alcohol. The polymerized furfuryl alcohol in the brown sample was then changed to black carbon by carbonization at 823 K for 3 h in vacuo. The sample was subsequently crystallized by heating in a He atmosphere at 923 K for 2 h. The carbon template in the crystallized sample was then removed by calcination at 773 K for 15 h in air. Powder XRD patterns were obtained on a Rigaku RINT 2100 diffractometer with $Cu_{K\alpha}$ radiation. TEM images, ED patterns and EDX were obtained using a 200 kV JEOL JEM2010F microscope. N_2 sorption isotherms were measured using SA-3100 systems, and pore-size distributions were determined by Barett-Joyner-Halenda (BJH) analysis.

Received: September 30, 2002
Revised: March 13, 2002 [Z50263]

Keywords: crystal engineering · mesoporous materials · nanostructures · niobium · tantalum

[1] F. Schüth, *Chem. Mater.* **2001**, *13*, 3184 – 3195.
[2] P. Yang, D. Zhao, D. I. Margolese, B. F. Chemelka, G. D. Stucky, *Chem. Mater.* **1999**, *11*, 2813 – 2826; U. Ciesla, F. Schüth, *Microporous Mesoporous Mater.* **1999**, *27*, 131 – 149.
[3] Y. Takahara, J. N. Kondo, T. Takata, D. Lu, K. Domen, *Chem. Mater.* **2001**, *31*, 1194 – 1199.
[4] M. Uchida, J. N. Kondo, D. Lu, K. Domen, *Chem. Lett.* **2002**, 498 – 499.
[5] G.-J. Li, S. Kawi, *Talanta* **1998**, *45*, 759 – 766; T. Hyodo, N. Nishida, Y. Shimizu, M. Egashira, *Sens. Actuators B* **2002**, 209 – 215; F. Chen, M. Liu, *Chem. Commun.* **2000**, 2095 – 2096.
[6] S. Inagaki, S. Guan, T. Ohsuna, O. Terasaki, *Nature* **2002**, *416*, 304 – 307.
[7] I. Schmidt, A. Boisen, E. Gustavsson, K. Stahl, S. Pehrson, S. Dahl, A. Carlsson, C. J. H. Jacobsen, *Chem. Mater.* **2001**, *13*, 4416 – 4418; C. J. H. Jacobsen, C. Madsen, J. Houzvicka, I. Schmidt, A. Carlsson, *J. Am. Chem. Soc.* **2000**, *122*, 7116 – 7117.
[8] B. Lee, D. Lu, J. N. Kondo, K. Domen, *Chem. Commun.* **2001**, 2118 – 2119; B. Lee, T. Yamashita, D. Lu, J. N. Kondo, K. Domen, *Chem. Mater.* **2002**, *14*, 867 – 875.
[9] T. Katou, J. N. Kondo, D. Lu, K. Domen, *J. Mater. Chem.* **2002**, *12*, 1480 – 1483.
[10] T. Katou, B. Lee, D. Lu, J. N. Kondo, M. Hara, K. Domen, unpublished results.
[11] S. Jun, S. H. Joo, R. Ryoo, M. Kurk, M. Jaroniec, Z. Liu, T. Ohsuna, O. Terasaki, *J. Am. Chem. Soc.* **2000**, *122*, 10712 – 10713; M. Kurk, M. Jaroniec, R. Ryoo, S. H. Joo, *.J. Phys. Chem. B* **2000**, *104*, 7960 – 7968; S. H. Joo, S. J. Choi, I. Oh, J. Kwak, Z. Liu, O. Terasaki, R. Ryoo, *Nature* **2001**, *412*, 169 – 172.
[12] M. Kang, S. H. Yi, H. I. Lee, J. E. Yie, J. M. Kim, *Chem. Commun.* **2002**, 1944 – 1945; A. H. Lu, W. Schmidt, A. Taguchi, B. Spliethoff, B. Tesche, F. Schüth, *Angew. Chem.* **2002**, *114*, 3639 – 3642; *Angew. Chem. Int. Ed.* **2002**, *41*, 3489 – 3492.

